
## Apatite Cluster in Zambian Emerald

This author recently studied a 1.68 ct faceted emerald containing several inclusions, including blocky fluid inclusions, transparent brownish crystals, needles, and particle clouds. These inclusions as well as the trace element chemistry supported a Zambian geographic origin. The emerald also exhibited elongated transparent crystals that resembled amphibole. In this case, Raman spectroscopy confirmed the mineral as apatite. Interestingly, this apatite formed a distinct inclusion cluster consisting of a large hexagonal prismatic crystal (a morphology typical of the mineral) associated with a multitude of rod- and bamboo-shaped crystals in various directions (figure 1). Other solid crystals observed in Zambian emerald include mica, actinolite (amphibole), quartz, zircon, and chromite.

Apatite, a common phosphate mineral, has previously been reported in various forms and in many other types of gems such as corundum, spinel, feldspar, and garnet, and it is not surprising to find it in emerald. However, this is the first time the author has encountered this fantastic form of apatite in emerald.

*Ungkhana Atikarnsakul*
*GIA, Bangkok*

## Blue Apatite in Tanzanian Garnet

In the micro-world, it can be challenging to identify inclusions based on sight alone, as many minerals can have a similar appearance. Occasionally, though, some inclusions have characteristic features that can aid in their identification.

Recently this author had the opportunity to observe a pyrope-spessartine garnet, reportedly from Lindi Province, Tanzania, that contained blue crystal inclusions ensconced among intersecting needles (figure 2). Analysis with micro-Raman spectroscopy identified the inclusions as apatite. Apatites are known for their bright blue hues, and these inclusions offered an attractive example.

*Figure 1. An inclusion cluster consisting of a hexagonal prismatic apatite crystal and many rod- and bamboo-shaped crystals of apatite in a Zambian emerald. Photomicrograph by Ungkhana Atikarnsakul; field of view 3.60 mm.*

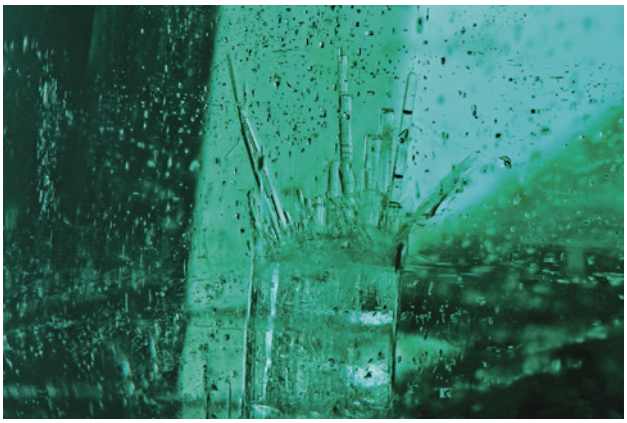

*About the banner: The surface of this synthetic amethyst shows a multitude of rhombohedral crystal faces. Photomicrograph by Nathan Renfro; field of view 15.67 mm.*

Gems & Gemology, Vol. 58, No. 2, pp. 226–233.
© 2022 Gemological Institute of America

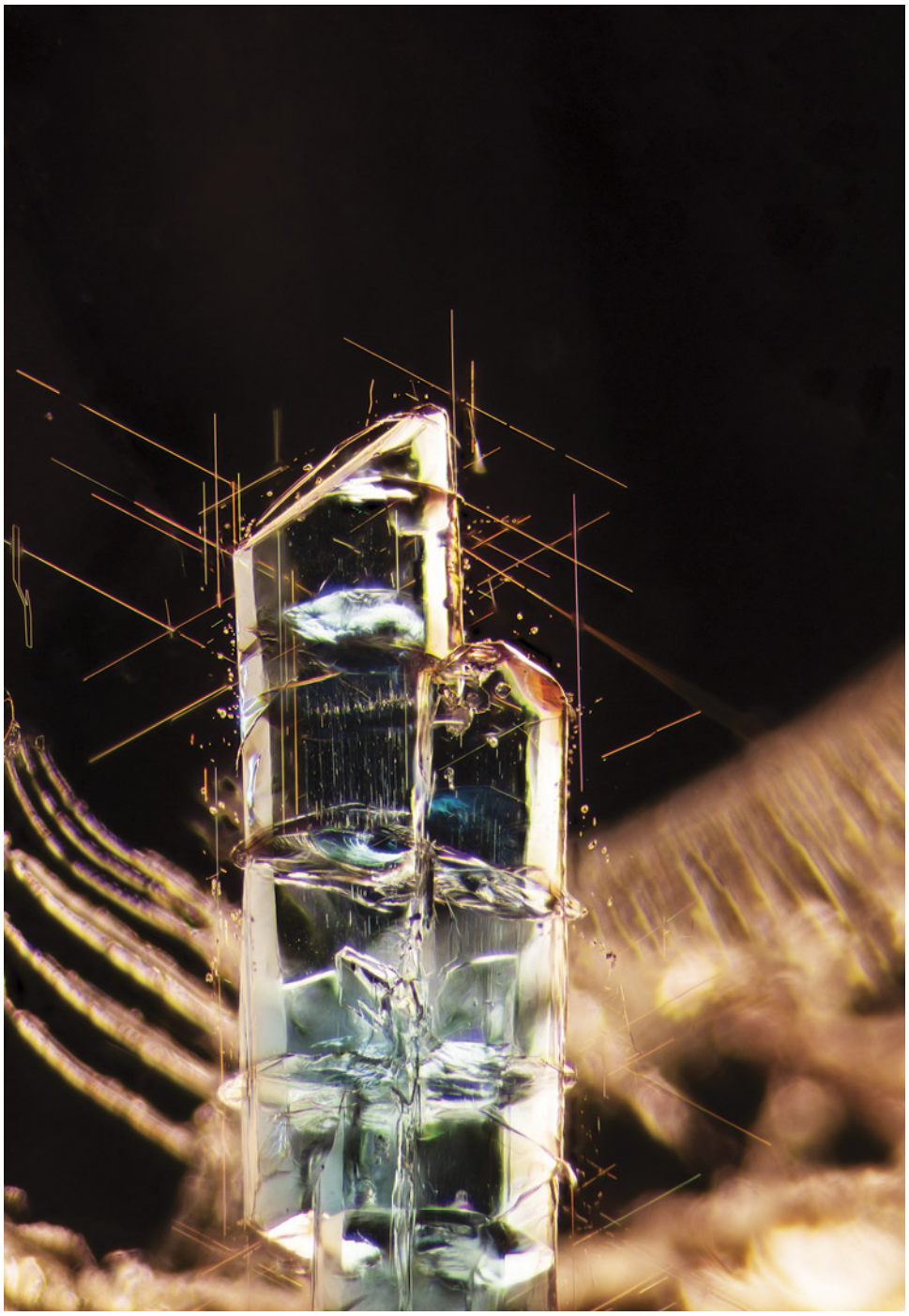

*Figure 2. Blue apatite crystals are beautifully framed by prominent rutile needles in a garnet from Tanzania. Photomicrograph by E. Billie Hughes; field of view 3.5 mm.*

While this sample hails from Tanzania, blue apatite has previously been reported as an inclusion in garnet from Madagascar (Winter 2020 *G&G* Micro-World, p. 526). These inclusions' distinctive appearance may help gemologists recognize the material in other samples, but further analysis should be performed to identify them definitively.

*E. Billie Hughes*
*Lotus Gemology, Bangkok*

## Large Diamond Inclusion in Diamond

Recently, the authors examined a 2.01 ct Faint green round brilliant diamond with a fascinating diamond crystal inclusion that displayed a transparent, ghost-like appearance. Due to the large size of this nearly invisible crystal, the stone was given a clarity grade of $SI_2$.

Photomicrography was used to document the features of this inclusion. Triangular etch features, also known as

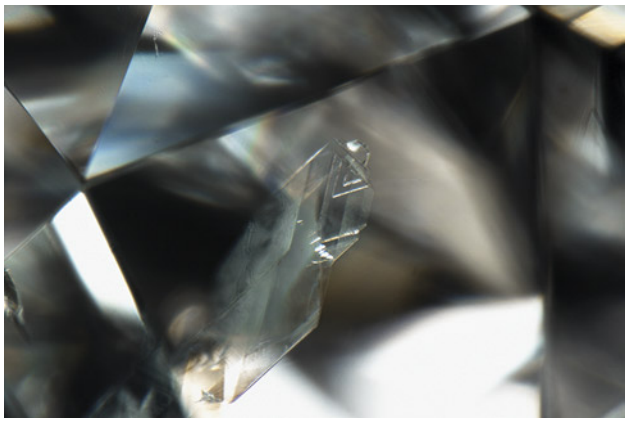

*Figure 3. Trigons seen on a diamond crystal inclusion visible through the crown of a round brilliant diamond. Photomicrograph by A'Dhi Lall; field of view 2.11 mm.*

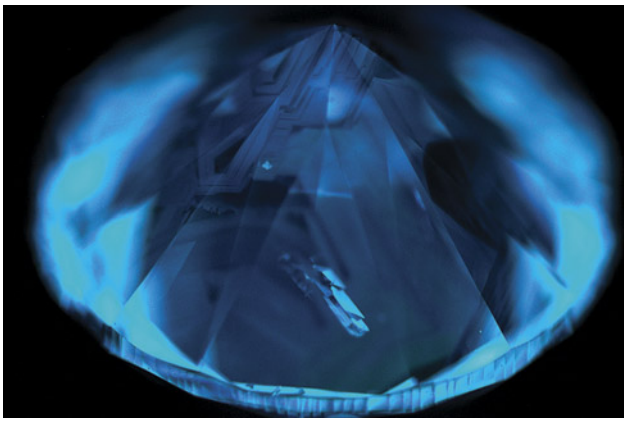

*Figure 5. DiamondView image of the diamond inclusion in the diamond host. Image by Luthfia Syarbaini.*

trigons, were seen on the inclusion (figure 3). These are typically natural growth markings of diamonds, confirming the inclusion as diamond. The diamond crystal inclusion appeared to have sharp and easily recognizable faces. Images with cross-polarized light show strain between the inclusion and the host diamond (figure 4). A DiamondView image also reveals the diamond crystal inclusion (figure 5).

Generally, the beauty and value of a diamond increase with the absence of inclusions. Yet the presence of a diamond inclusion gave this diamond a certain distinction, which in the authors' opinion added to its beauty and value.

*Luthfia Syarbaini, A'Dhi Lall, and Paul Johnson*
*GIA, New York*

## Natural Diamond with Extensive Network of Etch Channels

The authors recently examined a 5.19 ct type IIa natural diamond (figure 6) displaying numerous etch channels (figure 7). Etch channels are open tubes whose formation is related to dissolution processes within the stone. They form due to the dissolution of dislocations inside the crystal during or after growth and can result in various patterns; most commonly, they form as trigons or rarely as channels that appear as parallel lines, zigzags, or "worm-like" structures (T. Lu et al., "Observation of etch channels in several natural diamonds," *Diamond and Related Materials*, Vol. 10, 2001, pp. 68–75, and references therein; Spring 2018 *G&G*

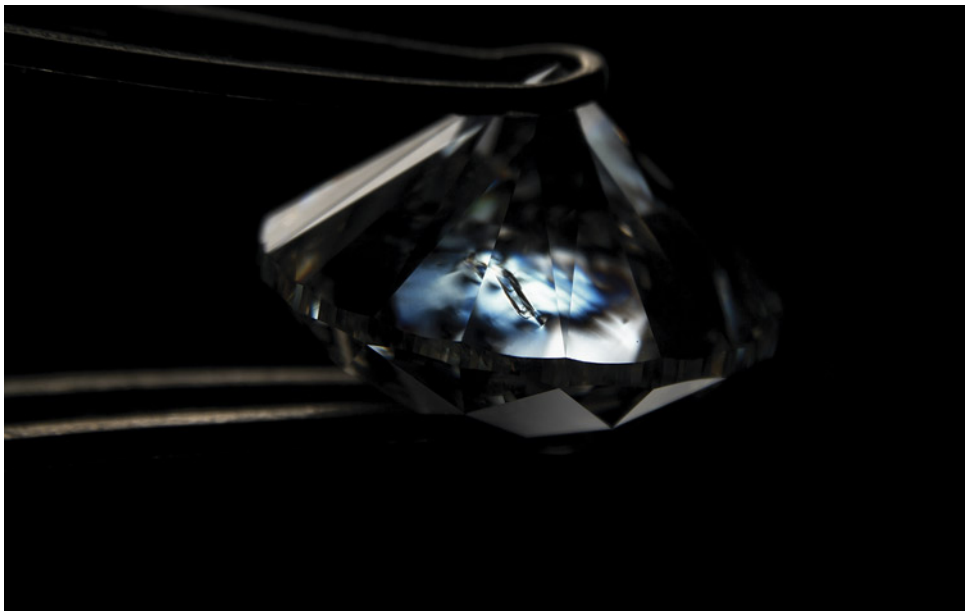

*Figure 4. Strain between the host diamond and the diamond inclusion is revealed by the interference colors in cross-polarized light. Photomicrograph by A'Dhi Lall; field of view 13.55 mm.*

*Figure 6. This 5.19 ct diamond with I color and $I_2$ clarity displays numerous etch channels visible to the eye. Photo by Annie Haynes.*

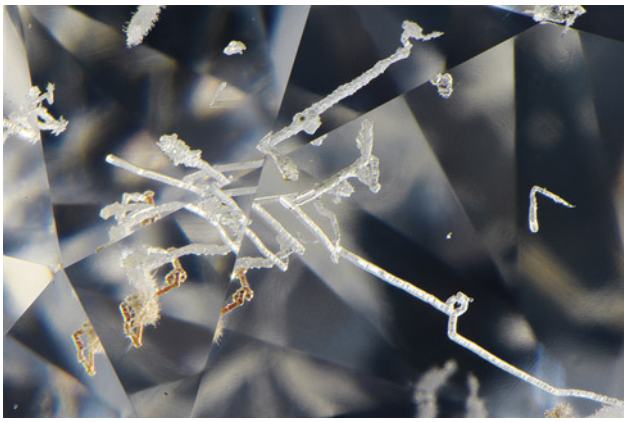

*Figure 7. A network of natural etch channels gives this diamond a distinctive appearance. Most of the channels have a width of ~100–150 µm, while some (e.g., lower left) show evidence of brown radiation stains. Photomicrograph by Nathan Renfro; field of view 4.69 mm.*

Micro-World, pp. 66–67). Etch channels terminate at typically rhombic openings visible at the surface of the stone (Spring 2018 *G&G* Micro-World, pp. 66–67). The extensive network of etch channels in this diamond resulted in an $I_2$ clarity grade.

Photoluminescence (PL) mapping using 455 and 532 nm laser excitation (figures 8 and 9) revealed an increase in the GR1, 3H, and TR12 centers along the walls of the etch channels; all of these centers are defects associated with radiation exposure. The nitrogen vacancy centers $NV^0$ (zero-phonon line [ZPL] at 575 nm) and $NV^-$ (ZPL at 637

*Figure 8. Left: False-color map showing the peak area intensity of the radiation-related TR12 center (ZPL at 469.9 nm); this 455 nm PL map was compiled from 18,768 spectra collected at 45 µm pixel size. Right: The false-color map overlain with a reflected light image of the table facet. Most of the etch channels seen in the false-color map correspond with an opening observed on the table.*

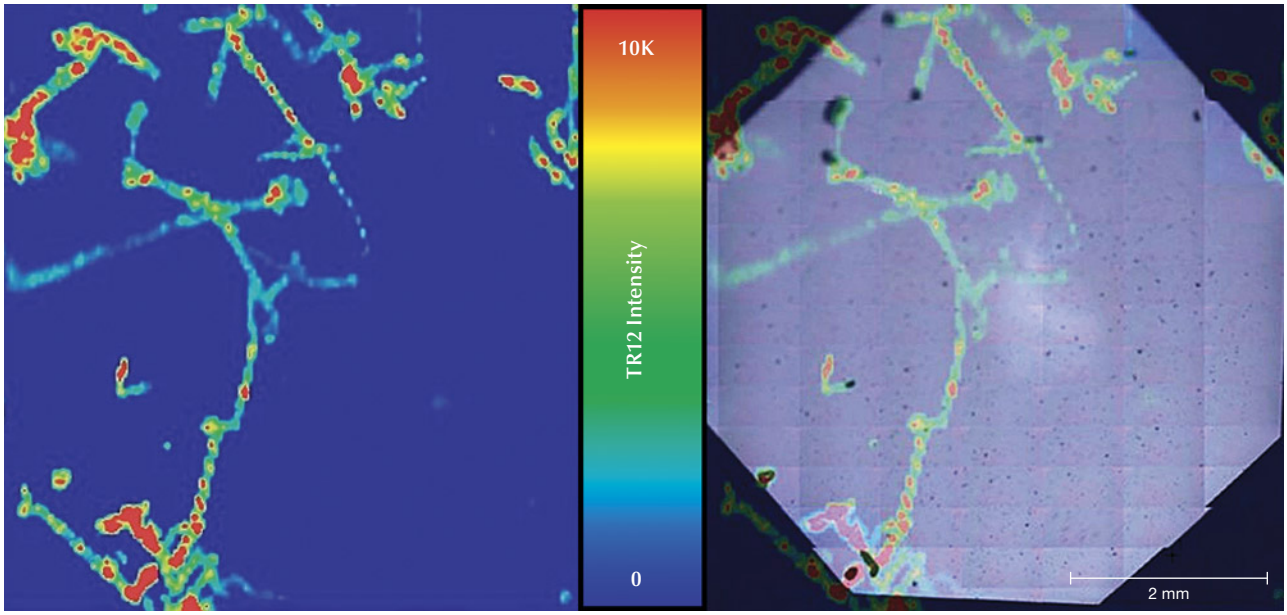

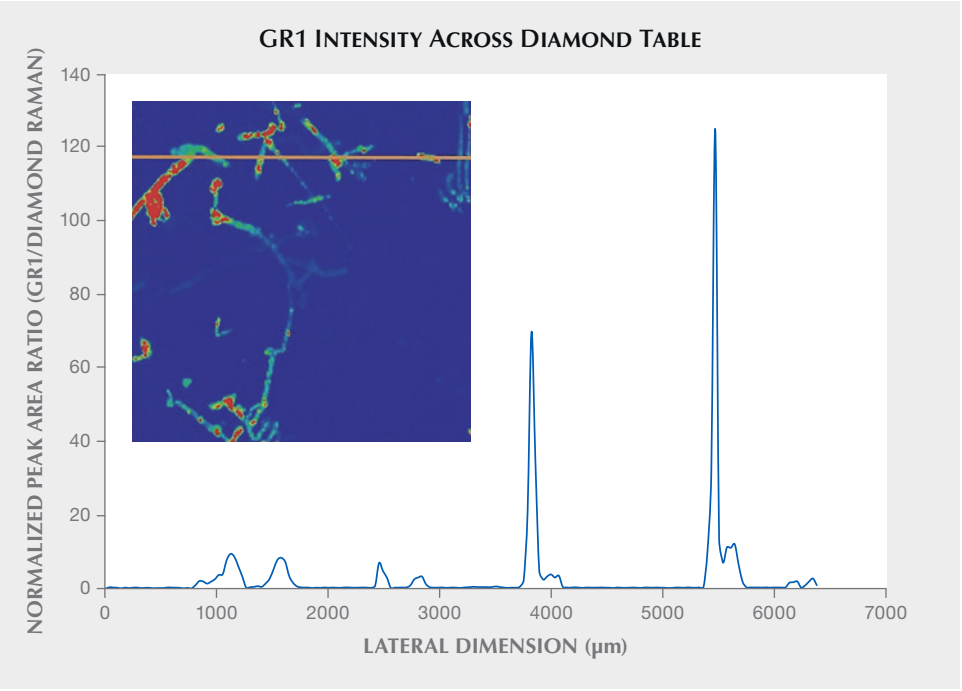


*Figure 9. GR1/Raman peak area ratios calculated from the 532 nm PL map (inset) cutting across multiple channels along the orange line. Higher GR1/Raman areas are concentrated along the etch channels.*

nm) were also concentrated along these channels. The concentration of these defects along the etch channels suggests that radioactive fluids once flowed through the tubes. The radioactive fluids had an impact on the areas in direct contact, creating elevated concentrations of radiation-related peaks. Other prominent PL peaks along the cavities were centered at 474, 598.75, and 461.5 nm. The radiation in these fluids would have been low enough to not create much observable staining, as patches of green to brown color associated with radiation staining were not observed in most of the etch channels. However, there were some isolated spots of green radiation stains and some channels with a brownish appearance (figure 7) and elevated concentrations of radiation-related features (figures 8 and 9). Additionally, the exposure to radioactive fluids must have occurred after the diamond was brought to the near-surface region following kimberlite eruption, as these radiation-related features would not withstand the high temperatures within the mantle.

Similar radiation features have previously been observed in another stone with cavities (Spring 2020 Lab Notes, pp. 126–127), but to a much lesser degree. The extensive network of etch channels within this diamond is one more example of the extraordinary possibilities within the natural world.

*Taryn Linzmeyer and Sally Eaton-Magaña*
*GIA, Carlsbad*

## Eye Pattern in a Rock Fragment

Recently, the authors encountered a partially polished rock fragment measuring 14.50 × 9.43 × 2.43 mm and weighing 3.45 ct that exhibited a very realistic eye pattern (figure 10). Various shades of yellow and green material formed the pupil and iris, while a distinctive white outline surrounded the iris as a sclera. Microscopic observation revealed different microcrystalline minerals. Raman spectroscopy identified pyroxene, feldspar, and quartz as the most abundant minerals. Energy-dispersive X-ray fluorescence (EDXRF) analysis revealed silicon as the dominant element, while traces of iron and potassium were also detected.

Naturally formed eye patterns in gems are rare but do exist, such as a "dragon's eye" in a fire agate (Winter 2015 *G&G* Micro-World, p. 441) and a radial eye structure in a sapphire (Summer 2017 *G&G* Micro-World, pp. 244–245). While the textures in rocks are much more diverse than those in single-mineral gemstones, observing such a unique feature is always exciting.

*Ching Yin Sin*
*GIA, Hong Kong*

*Piradee Siritheerakul*
*GIA, Bangkok*

## Fracture-Filled Emerald with Mysterious Filler Patterns

Emeralds are known to have natural cracks or fractures. The filling of surface-reaching fractures with various oils and resins is the most common practice to minimize fractures to improve an emerald's appearance. The author recently examined a 3.04 ct emerald that revealed a mysterious filler pattern along the fractures, resembling a

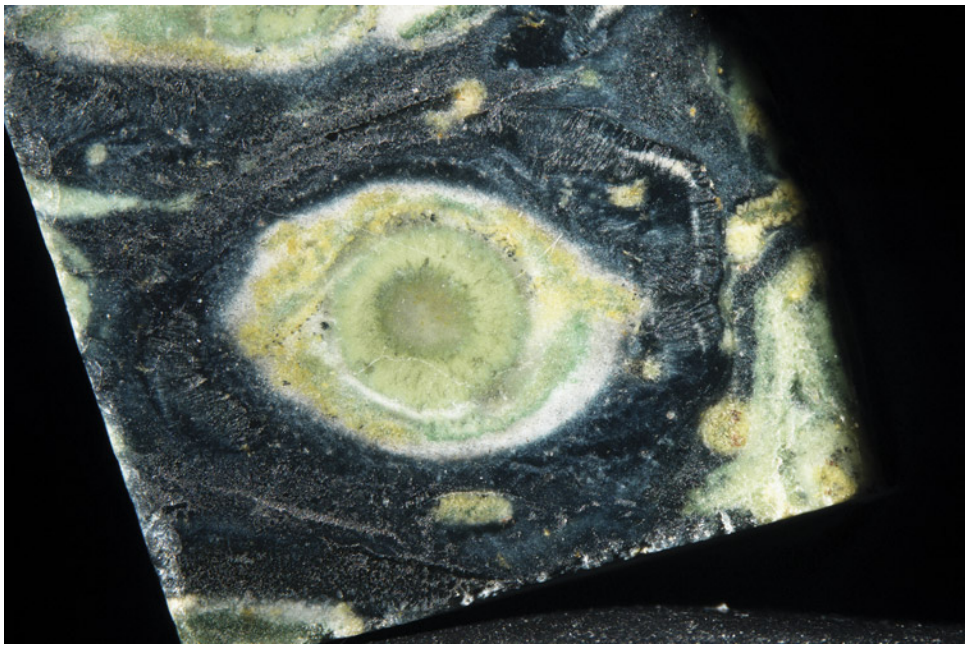

*Figure 10. An eye pattern complete with pupil, iris, and sclera is clearly visible in this rock fragment. Photomicrograph by Polthep Sukpanish; field of view 12.5 mm.*

labyrinth and convolution (figure 11). Fracture filling can be identified using various methods. In this case, it displayed a chalky fluorescence under long-wave ultraviolet flashlight and was also detected with simple microscopic observation and fiber-optic lighting. The internal graining, irregular two-phase inclusions, and long needles within this stone indicated a natural origin. This was a unique and visually interesting pattern in the fracture filling material of an emerald.

*Ungkhana Atikarnsakul*
*GIA, Bangkok*

## Flux-Grown Synthetic Beryl Overgrowth

Most of the synthetic beryl currently on the market has been created by a hydrothermal process. Hydrothermally grown crystals have obviously different crystal forms compared to their natural counterparts. Hydrothermal synthetics are often easily identified by their typical zigzag- or chevron-patterned graining and color zoning. Flux-grown synthetics, though less common, are able to form more natural-looking crystals. However, despite having natural forms, flux synthetics contain many unusual inclusions that clearly distinguish them from their natural counter-

*Figure 11. Emerald filler with labyrinth- and convolution-like pattern. Photomicrographs by Ungkhana Atikarnsakul; fields of view 2.0 mm (left) and 2.7 mm (right).*

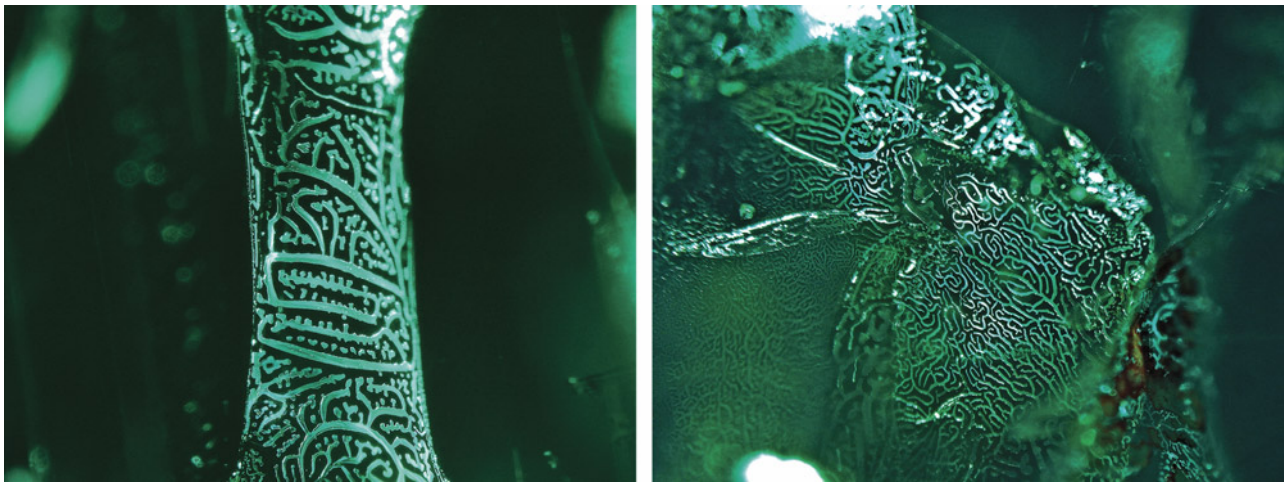

*Figure 12. Doubly terminated flux synthetic beryl crystal, measuring 32.45 × 30.36 × 25.29 mm. Photo by Annie L. Haynes.*

parts. Copper platelets that form within the crystal either from contamination or intentionally introducing metal in the growth material are obvious indications of synthetic origin. Flux fingerprints are another easily observed type of inclusion unique to flux synthetic crystals.

Weighing 211.78 ct, the hexagonal doubly terminated crystal in figure 12 looks like a natural beryl crystal at first glance. Eye-visible well-formed copper platelets and wispy flux fingerprints indicate that the stone did not form naturally. A closer look revealed reddish clouds of well-formed minute copper platelets and copper crystals. Euhedral red rod-like crystals of columbite were scattered throughout, similar to those in a natural sample. Partially healed tension cracks with white secondary flux particles were also present. A few areas throughout the crystal had unique thin angular and jagged films containing blue flux liquid and gas bubbles (figure 13). Areas with higher clarity reveal the boundary between the natural aquamarine seed crystal and the flux overgrowth. This stone is a product of synthetic flux beryl overgrowth on a natural aquamarine seed crystal produced in a Russian synthetic gem facility.

*Jamie Price*
*GIA, Carlsbad*

## "Boomerang" Inclusion in a Rough Topaz

A 21.46 ct colorless rough topaz was recently submitted to Taiwan Union Lab of Gem Research (TULAB) for identification service. Microscopic observation showed a few prismatic brown inclusions with submetallic luster. One of the inclusions was a unique twinned crystal composed of two

*Figure 13. A suite of columbite rods, copper crystals, and a large air bubble seen within a film of blue flux liquid. Photomicrograph by Jamie Price; field of view 7.19 mm.*

prismatic crystals forming a 120° intersection angle. With its shape and backdrop, the twinned crystal resembled a boomerang flying across the sky (figure 14). This inclusion was later confirmed to be tantalite-(Mn), based on Raman spectroscopy and comparison with the RRUFF database. Polarized light and reflected illumination were adopted to reduce doubling and obtain clearer photomicrographs, and the images were processed to extend depth of field.

*Shu-Hong Lin*
*Institute of Earth Sciences,*
*National Taiwan Ocean University*
*Taiwan Union Lab of Gem Research, Taipei*

*Tsung-Ying Yang, Kai-Yun Huang, and Yu-Shan Chou*
*Taiwan Union Lab of Gem Research, Taipei*

*Figure 14. The "boomerang" inclusion in this topaz was confirmed by Raman spectroscopy to be a twinned crystal of tantalite-(Mn). Photomicrograph by Shu-Hong Lin; field of view 0.71 mm.*

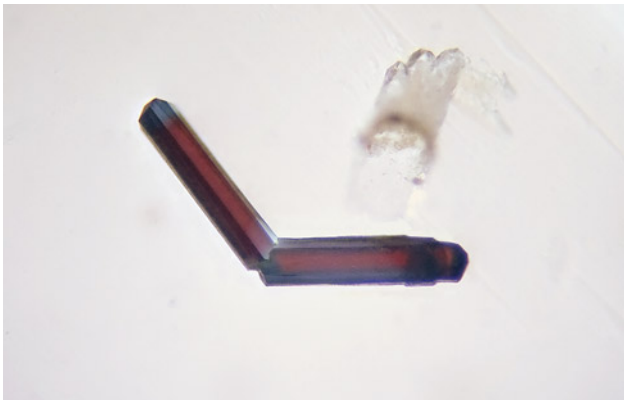

*Figure 15. Several bright red to dark red well-formed trigonal crystals of cinnabar highlight the interior of the fluorite crystals in this fluorite and calcite cluster from Spain. Photo by Diego Sanchez.*

## Quarterly Crystal: Cinnabar in Fluorite

This issue's Quarterly Crystal deals with a 362.09 ct crystal cluster of fluorite and calcite recently examined by the authors. The 55.79 × 42.80 × 38.63 mm specimen was colorless and transparent to translucent and played host to several small bright red to dark red well-formed trigonal crystals, visible in figure 15. These crystals were all situated on the same growth plane in the fluorite portion.

The fluorite and calcite specimen was obtained from Jordi Fabre of Fabre Minerals in Barcelona. It is from the Emilio mine in the Caravia mining area in the Asturias region of northwestern Spain. The Emilio mine is known to produce fluorite crystals with inclusions of various sulfides, including cinnabar. Therefore, the pure red bodycolor of these inclusions, together with the trigonal symmetry shown in figure 16, strongly suggested they were cinnabar. Using Raman microspectrometry, we were able to identify the inclusions as cinnabar, thereby confirming our initial impression.

*John I. Koivula and Nathan Renfro*
*GIA, Carlsbad*

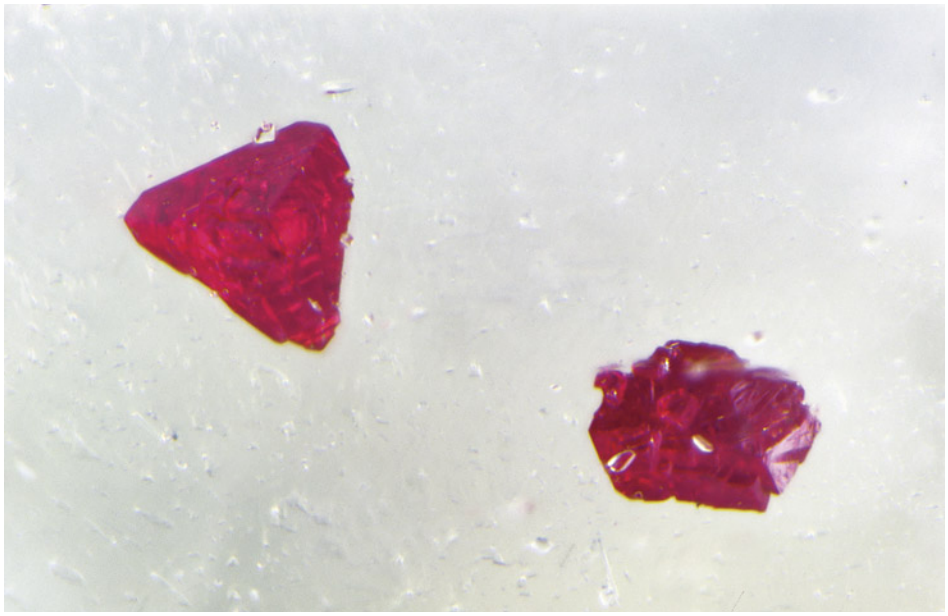

*Figure 16. A combination of optical microscopy and Raman analysis served to identify the trigonal inclusions as the mercury sulfide cinnabar. Photomicrograph by Nathan Renfro; field of view 2.35 mm.*